Influence of Imbalance of Earth-pressure on Wall Deflections on a Deep Excavation

L.W. WONG & Y.N. HO
SMEC Asia Limited

doi: https://doi.org/10.21467/proceedings.7.7.28

ABSTRACT

An undersea vehicular tunnel was constructed by using the cut-and-cover method. The cofferdam supporting the excavation of 35 m maximum in depth and 50 m in width comprised intermittent pipe pile walls of 50 m maximum in depth. The struts were preloaded to the magnitudes as large as 16.4 MN. Due to the difference in the depths to the rockhead levels on both sides of the cofferdam, there is the earth-pressure imbalance effect causing differential lateral wall deflections. The wall on the shallower rockhead side was pushed back by the wall on the opposite side with deeper rockhead levels through the struts. The wall deflections were as large as 194 mm on one side and 22 mm on the opposite side. As a result, the central axis of the excavation trench shifted by as large as 156 mm. The magnitude of shifting of the central axis is proportional to the ratio of the depths to the rockhead on the two sides of the excavation.

Keywords: Wall deflections, Cut-and-cover tunnel, Earth-pressure imbalance, struts preloading.

1 INTRODUCTION

The earth-pressure imbalance effects causing different in wall deflections of deep excavation cases have been reported by the researchers. Moh & Hwang (1997) reported the asymmetrical wall deflections at a basement excavation case located at the northern rim of the Taipei basin. Wong & Yong (2013) reported the earth-pressure imbalance effects for an excavation case for the Central Wanchai Bypass (CWB) cut-and-cover tunnel. In the numerical analysis, the half model assuming the central axis as a fixed boundary along the horizontal direction has often been adopted. The occurrence of the earth pressure imbalance would lead to under-estimation of the wall deflections on one side and over-estimation of those on the opposite side.

The excavation for a 500 m length of a dual-3 lanes vehicular undersea tunnel was constructed by using the cut-and-cover method. The excavation as deep as 35 m was supported by intermittent pipe pile walls on the north and the south sides. The horizontal inward wall deflections as large as 194 mm on the south wall occurred in the final excavation stage. On the opposite side along the north wall, the outward wall deflection as large as 160 mm occurred. The central axis of the excavation trench shifted northward by around 156 mm. In order to understand the mechanism causing the asymmetrical wall deflections and to improve the effectiveness on the design and construction of the infrastructure works, the undersea tunnel case on earth pressure imbalance is critically studied.

2 HYDROGEOLOGICAL CONDITIONS

2.1 Extent of undersea tunnel

The undersea tunnel accommodating the dual-3 carriageways is located on the north shore of the Victoria Harbour. Descending from the ground level of 5 mPD at the at-grade section, the undersea tunnel section has the lowest formation level around -32 mPD. As depicted in Figure 1, the undersea tunnel presented in this paper

© 2025 Copyright held by the author(s). Published by AIJR Publisher in "Proceedings of The HKIE Geotechnical Division 45th Annual Seminar 2025 - Advancing Geotechnical Practice: Sustainable Solutions to Land & Infrastructure Developments" (GDAS2025). Organized by the Geotechnical Division, The Hong Kong Institution of Engineers, Hong Kong on May 09, 2025.

Proceedings DOI: 10.21467/proceedings.7.7; Series: AIJR Proceedings; ISSN: 2582-3922; ISBN: 978-81-989164-3-3

is 50 m in width and 230 m in length. Eight inclinometers were installed immediately behind the pipe pile walls along 4 monitoring sections. The piezometers were installed near Sections 11 and 12.

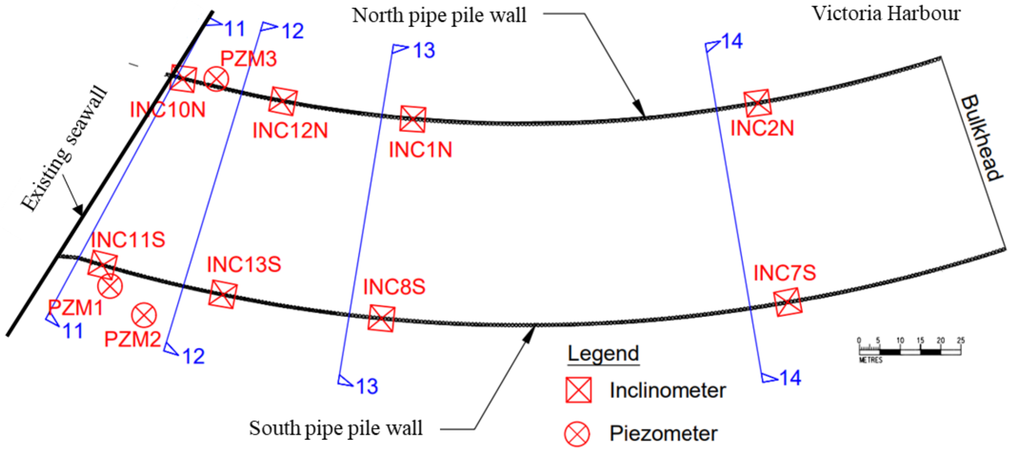

Figure 1: Plan of undersea tunnel showing the locations of the instruments

2.2 Subsoil conditions

The subsoils along the tunnel route mainly comprise the marine deposits, the alluvium, the granitic saprolites and the granite bedrock. The seabed level was around -5 mPD. The rockhead levels along the route alignment vary from -22 mPD to -50 mPD. Along the shoreline, there is a fill layer of approximately 7 m in thickness. Figure 2 depicts the soil and rock profiles along the longitudinal direction of the tunnel.

The fill layer overlies the marine deposits clay of 5 m thick, which is underlain by the Quaternary alluvial silty sand of 12 m average in thickness. The alluvium is underlain by the saprolite of completely decomposed granite (Granite V) of 13 m average in thickness and the highly decomposed granite (Granite IV) of 10 m maximum in thickness. The bedrock of moderately decomposed to slightly decomposed granite (Granite III/II) is encountered at elevations ranging from -33 mPD to -68 mPD. The soil and rock conditions at the project site is summarized in Table 1. The mean sea level is 1.2 mPD. The tide level of 2.8 mPD was allowed for the cut-and-cover tunnel construction.

Table 1. Summary of soil profile along the undersea tunnel

Soil strata	Top level, mPD	N value	Description
Fill	4	5 to 12	Greyish silty SAND
Marine deposits	-5	5	Dark grey silty CLAY
Alluvium	-10	11 to 40	Stiff yellowish brown silty SAND
Granite V	-20	28 to 80	Yellowish to reddish brown silty SAND
Granite IV	-50 to -60	90 to 160	Yellowish brown sandy GRAVEL and cobbles
Granite III/II	-33 to -68	-	Pink to brown medium to coarse grained Granite

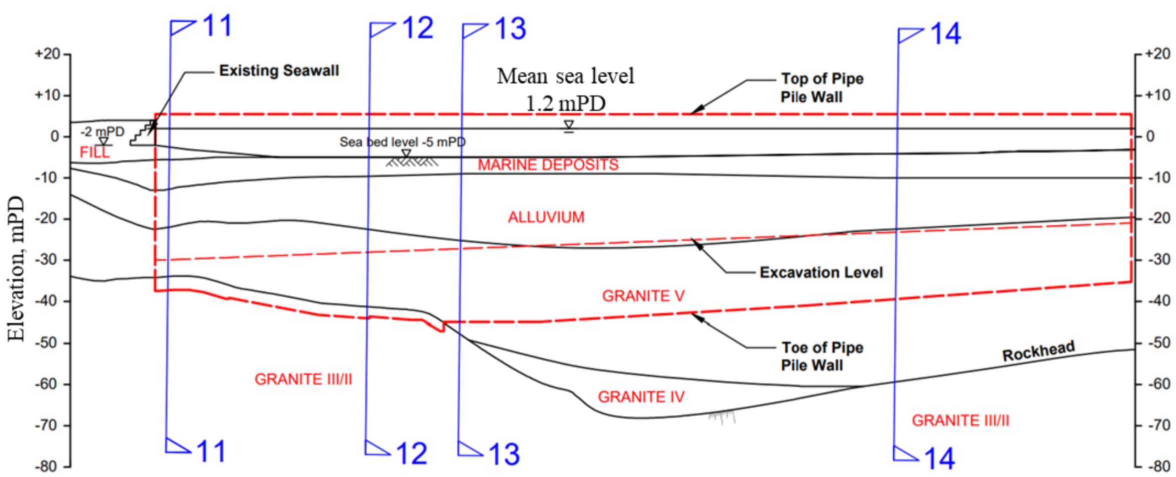

Figure 2: Soil and rock profile along longitudinal section of the cut-and-cover tunnel

2.3 Cofferdam for cut-and-cover construction

As depicted in Figure 3, the tunnel was constructed by using the bottom-up method. The excavation was supported by the intermittent pipe pile walls on the north and the south sides. These walls served as the cofferdam over the sea. The pipe piles had interlocking joints similar to those for sheet piles.

The intermittent pipe pile walls were composed of tubular steel sections of 813 mm in diameter, 16 mm in thickness and spacing at 900 mm. At Section 11 and Section 12, where the excavation depths exceeding 33 m, the pipe piles were strengthened by inserting steel H-section of UB 305 x 305 x 238 kg/m. The stiffnesses of the pipe pile wall, the EI values, were 100 MNm/m and 73 MNm/m for the sections with and without the H-pile insertion respectively. Such stiffnesses are equivalent to the EI value of 93 MNm/m for a concrete diaphragm wall of 0.4 m in thickness allowing a 0.7 reduction factor for cracks in concrete.

The cofferdam was supported with 5 to 9 levels of steel struts. The width of the excavation was 49 m. With the wall top level around 5.5 mPD and the toe levels ranging from -37 mPD to -47.5 mPD, the pipe pile walls were embedded 1.5 m to 7 m into Granite III/II.

The rockhead levels along the south wall are lower than those along the north wall. As summarized in Table 2, the rockhead levels between the north and the south pipe pile walls differ by as large as 9.5 m at Section 12. There were differences in the excavation levels on the north and the south sides. For example, the final excavation levels on the north and the south sides along Section 11 were -32.0 mPD and -31.5 mPD respectively.

Table 2: Embedment of the pipe pile wall and the inclinometers in rock

Section	Pipe pile wall	Rockhead level, mPD	Pipe pile wall		Inclinometer embedment			Final excavation level, mPD
			Toe level, mPD	Embedment in rock, m	Inclino-meter	Toe level, mPD	Embedment in rock, m	
11	North	-30.0	-37.0	7.0	INC10N	-36.2	6.2	-32.0
	South	-34.0	-39.0	5.0	INC11S	-38.2	4.2	-31.5
12	North	-32.0	-37.0	5.0	INC12N	-35.2	3.2	-30.6
	South	-41.5	-43.0	1.5	INC13S	-43.7	2.2	-29.5
13	North	-43.0	-47.5	4.5	INC1N	-63.7	20.7	-29.5
	South	-48.0	-45.0	-	INC8S	-55.7	7.7	-29.5
14	North	-59.0	-39.5	-	INC2N	-57.7	-1.3	-25.7
	South	-59.2	-37.5	-	INC7S	-61.2	2.0	-24.6

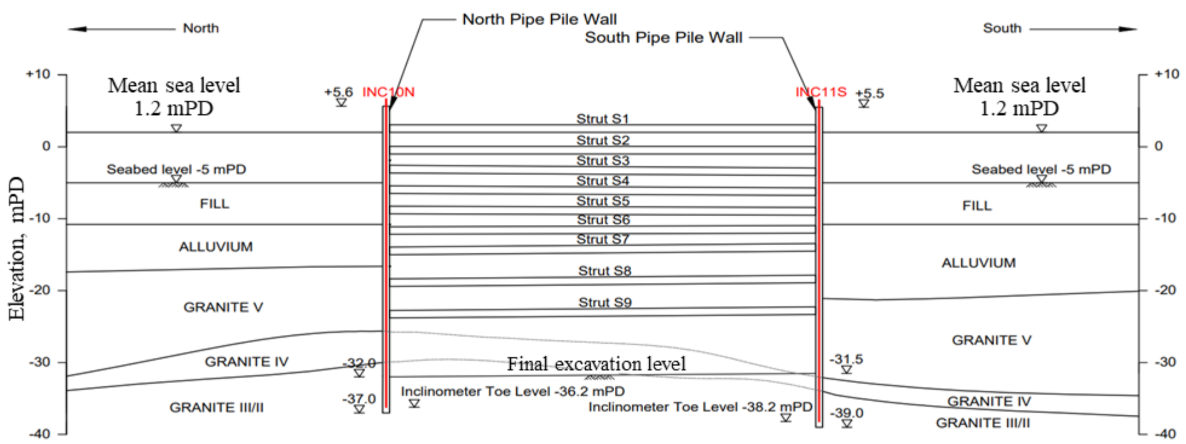

Figure 3: Soil and rock profile along Section 11 of the cut-and-cover tunnel

2.4 Groundwater conditions

As shown in Figure 1, piezometers PZM1 to PZM3 were installed behind the north and the south pipe pile walls in the vicinity of Section 11 and Section 12. Two piezometers were installed at each location. The upper piezometers were installed in the alluvium and the lower piezometers were in the Granite V stratum. Figures 4a and 4b present the variation of the piezometric levels on the south and the north sides of the excavation respectively. The daily readings show that the piezometric levels were under tidal influence with the average level around 1.2 mPD in the beginning stage of excavation.

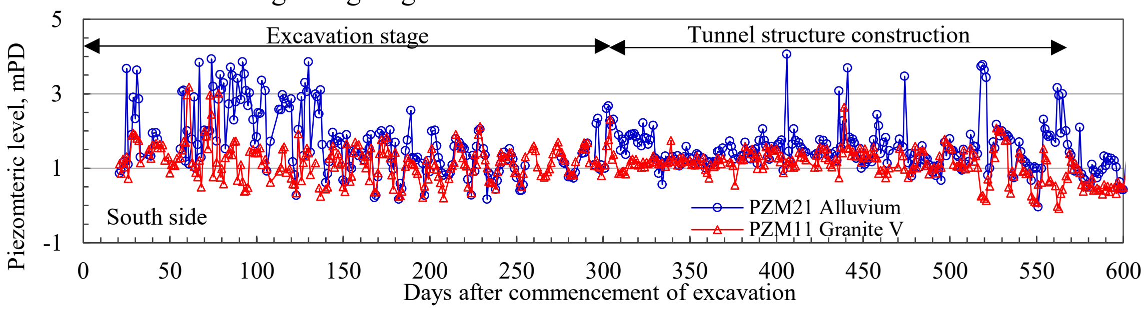

(a) Variation of piezometric levels behind the south pipe pile wall

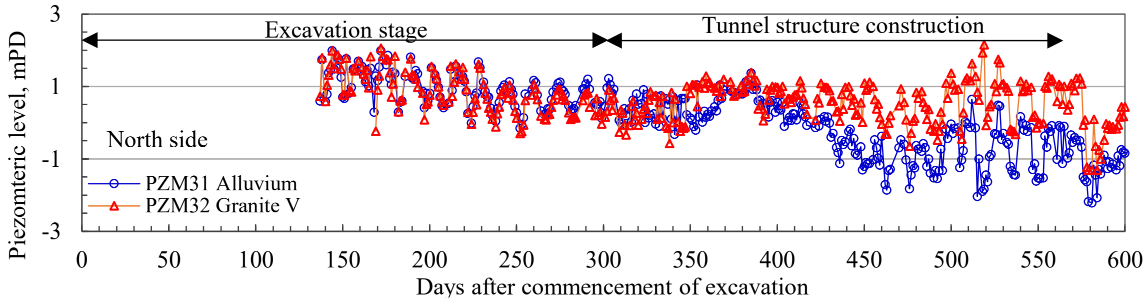

(b) Variation of piezometric levels behind the north pipe pile wall

Figure 4: Variation of the piezometric levels on both sides of Section 11

Figure 4a shows that on the south side of the cofferdam, the average piezometric levels in the alluvium layer were lowered from 1.5 mPD in the excavation stage to 1.0 mPD at the end of the tunnel structure construction stage. In the Granite V stratum, the average piezometric levels were gradually lowered from 1.5 mPD to 0.5 mPD during that period. The piezometric levels as high as 4.0 mPD observed in PZM21 were likely caused by the installation of the grout curtain behind the south pipe pile wall, where sensitive structures were located in the vicinity.

Figure 4b shows that on the north side of the cofferdam, the average piezometric levels in the alluvium layer were lowered from 1.2 mPD in the excavation stage to -1.0 mPD at the end of the tunnel structure construction stage. In the Granite V stratum, the average piezometric levels were gradually lowered from 1.2 mPD to 0 mPD during that period.

3 STRUTS INSTALLATION

3.1 Steel struts

Along Sections 12 to 14 of the tunnel, the twin-struts of level 1 and level 2 were fabricated into a steel truss of 4 m in height and 2.5 m in width. The level 1 twin-struts were the top chords and the level 2 twin-struts were the bottom chords of the steel truss. The upper chords comprised a pair of steel members of 914x4195x388 kg/m UB and the bottom chords comprised a pair of 914x305x289 kg/m UB. The steel trusses were erected at the bulkhead located at the east end of the cofferdam. After fabrication, the steel trusses of 46 m in span length were skidded one by one from east to west with the horizontal spacing around 8.5 m.

The struts below the level 2 were composed of twin-steel struts of 914x419x388 UB, which had the typical length of 12 m per segment. The twin-struts were installed by connecting the 12 m length modular segments with bolted joints. For the lowest struts S8 and S9 at Section 11, the twin struts were strengthened with steel plates of 25 mm in thickness.

Table 3 to Table 6 summarize the properties of the struts supporting the excavation at Section 11 to Section 14 along the undersea tunnel. The struts of 46 m in length were typically composed of 3 segments of 12 m in length and 2 segments with the knee braces at the strut-waling connections. There were 6 bolt connections, at the joints between the struts and waling segment and at those between the strut segments.

Table 3: Strut properties along Section 11

Strut levels	Elevation mPD	Depth, m	Steel member	Horizontal spacing, m	Preload, MN	Stage
S1	2.50	3.3	2-914x305x289 UB	7.0	-	1
S2	-0.50	6.3	2-914x419x388 UB		11.0	2
S3	-3.14	8.9	2-914x419x388 UB		13.7	3
S4	-5.98	11.8	2-914x419x388 UB		15.8	4
S5	-8.82	14.6	2-914x419x388 UB		15.8	5
S6	-11.66	17.5	2-914x419x388 UB		15.8	6
S7	-14.50	20.3	2-914x419x388 UB		15.8	7
S8	-18.90	24.7	2-914x419x388 UB & Plates		16.4	8
S9	-23.30	29.1	2-914x419x388 UB & Plates		16.4	9
Excavation	-32.00	34.5			-	10

Table 4: Strut properties along Section 12

Strut levels	Elevation mPD	Depth below sea level, m	Steel member	Horizontal spacing, m	Preload, MN	Stage
S1	2.50	0	2-914x419x388 UB	7.8	-	1
S2	-1.50	4.0	2-914x305x289 UB		-	2
S3	-5.40	7.9	2-914x419x388 UB		13.3	3
S4	-9.30	11.8	2-914x419x388 UB		14.0	4
S5	-12.50	15.0	2-914x419x388 UB		15.0	5
S6	-17.23	19.7	2-914x419x388 UB		15.0	6
S7	-23.90	26.4	2-914x419x388 UB		15.8	7
Excavation	-30.56	33.1			-	8

Table 5: Strut properties along Section 13

Strut levels	Elevation mPD	Depth below sea level, m	Steel member	Horizontal spacing, m	Preload, MN	Stage
S1	2.50	0	2-914x419x388 UB	8.4	-	1
S2	-1.50	4.0	2-914x305x289 UB		-	2
S3	-5.10	7.6	2-914x419x388 UB		13.5	3
S4	-8.90	11.4	2-914x419x388 UB		14.5	4
S5	-12.46	15.0	2-914x419x388 UB		14.8	5
S6	-16.21	18.7	2-914x419x388 UB		15.2	6
S7	-21.18	23.7	2-914x419x388 UB		15.2	7
Excavation	-29.73	32.2			-	8

Table 6: Strut properties along Section 14

Strut levels	Elevation mPD	Depth below sea level, m	Steel member	Horizontal spacing, m	Preload, MN	Stage
S1	2.00	0.5	2-914x419x388 UB	8.6	-	1
S2	-2.00	4.5	2-914x305x289 UB		-	2
S3	-6.62	9.1	2-914x419x388 UB		12.5	3
S4	-12.10	14.6	2-914x419x388 UB		15.8	4
S5	-20.00	22.5	2-914x419x388 UB		15.0	5
Excavation	-25.70	28.3				6

3.2 Struts preloading

Struts preloading was applied to the levels 2 to 9 struts along Section 11. For Sections 12 to 14, preloading was applied to the struts starting from level 3. Four hydraulic jacks were used for applying the design strut loads ranging from 11 MN to 16.4 MN. The jacking point was located near the mid portion of the strut. The preload was applied in 3 cycles. In Cycle 1, Cycle 2 and Cycle 3, the 50 %, 100 % and 110 % of the design strut load were applied. The extensions of the jack cylinders at the various applied loads and after their releasing were measured in each cycle. In the final Cycle 3, the applied load was locked-off by inserting a stack of shim plates to the gap at the jacking point between the north and the south strut segments. The thickness of each piece of shim plate ranged from 2 mm to 20 mm.

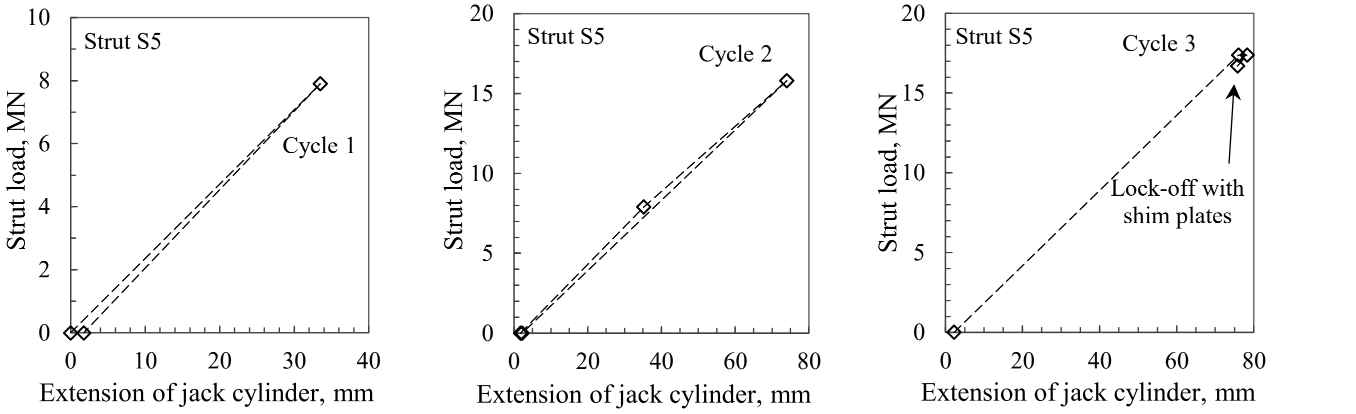

(a) Cycle 1 (b) Cycle 2 (c) Cycle 3

Figure 5: Load versus extension of jack cylinder for strut S5 along Section 11

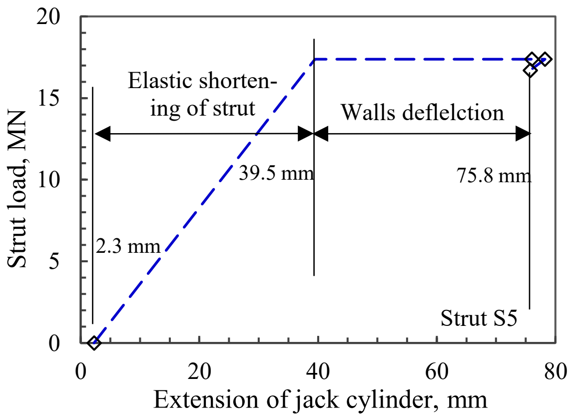

Figure 6: Deduction for walls deflection in Cycle 3 for strut S5 along Section 11

The jack cylinder extension measurements were conducted in the initial stage prior to apply loading, after jacking to the loads in each cycle and after releasing the applied loads. Figure 5 presents the applied loads versus the extensions of the jack cylinders for preloading the struts S5. It is noted that the skim plate has the minimum thickness of 2 mm. Gaps in the stack of shim plates less than 2 mm in width could not be filled up. After the shim plates were placed and the maximum load was released, the strut displacement reduced slightly due to closing of the gaps of less than 2 mm in width. As a result, although the struts were applied to 110 % during the preloading operation, the strut loads were locked-off to around 100 % of the design load after releasing the applied load. For strut S5, the shim plates inserted at the jacking point prior to releasing the applied load had the total thickness of 84 mm.

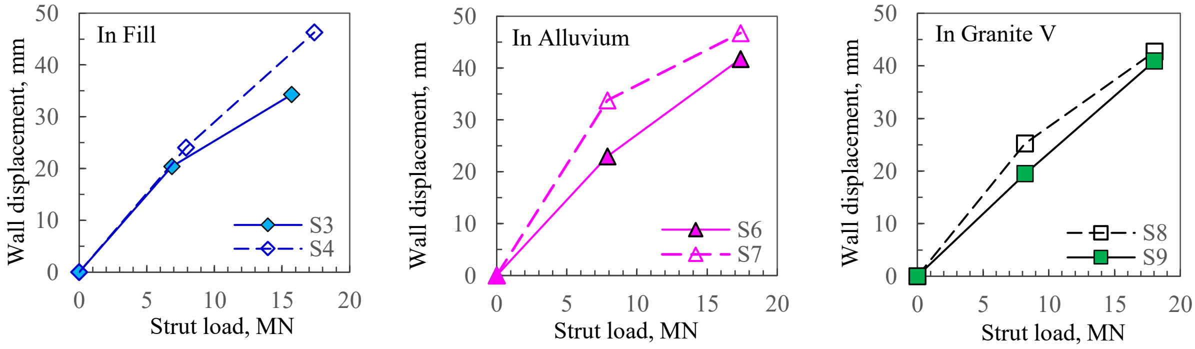

(a) Struts S3 and S4 (b) Struts S6 and S7 (c) Struts S8 and S9

Figure 7: Wall deflections caused by struts preloading at Section 11

3.3 Struts and wall displacements

The extension of the jack cylinder measured comprised 2 portions, the elastic shortening of the steel strut and the pushing back the supporting pipe pile walls under the preloading forces. As shown in Figure 6, using the elastic modulus of steel of 205 GPa and the sectional area of 988 cm^2 for the twin-strut, the elastic shortening of 39.5 mm for the strut S5 of 46 m in length at Section 11 is computed. The wall deflection of 38.8 mm at that strut level is deduced from the measured total extension of the jack cylinder of 78.3 mm. It is noted that the walls on both sides were pushed back by the strut at the same time.

The total wall deflections on 2 sides deduced from the load displacement curves in the various strut levels in the fill, the alluvium, in the Granite V strata are presented in Figure 7a to Figure 7c. The total wall deflections occurring at the north and the south walls due to the 110 % design strut loads ranged from 34 mm to 47 mm, with an average of 40 mm. There is not much difference in the wall deflections occurring between the fill, the alluvium and the Granite V strata, probably due to the fact that these 3 types of soil have similar stiffness values.

3.4 Wall displacements due to preloading observed by inclinometers

The wall deflections due to struts preloading are also assessed by the inclinometer readings. The magnitudes of wall deflections due to struts preloading have been deduced from the inclinometer profiles measured at 1 day prior to and 1 day after the preloading of the struts. The differences in wall deflections measured in these 2 days were the wall deflections caused by preloading the struts. Figure 8 presents the wall deflection profiles due to preloading struts S2 to S9. It is noted that the positive and the negative wall deflection values denote the southward and the northward wall movements respectively.

The wall deflections assessed by measuring the jack cylinder extensions during the struts preloading operation are consistent with those observed in the inclinometers 1-day after preloading. As summarized in Table 7, the relative wall deflections, the summation of the deflections measured in the north and the south walls, range 12 mm to 27 mm, with an average of 19 mm. Table 6 summarized that the wall deflections on the north wall and the south wall had the average of 13.9 mm and 5.1 mm respectively. The wall deflections occurring in the north wall contributed 3 quarter of the total wall deflections.

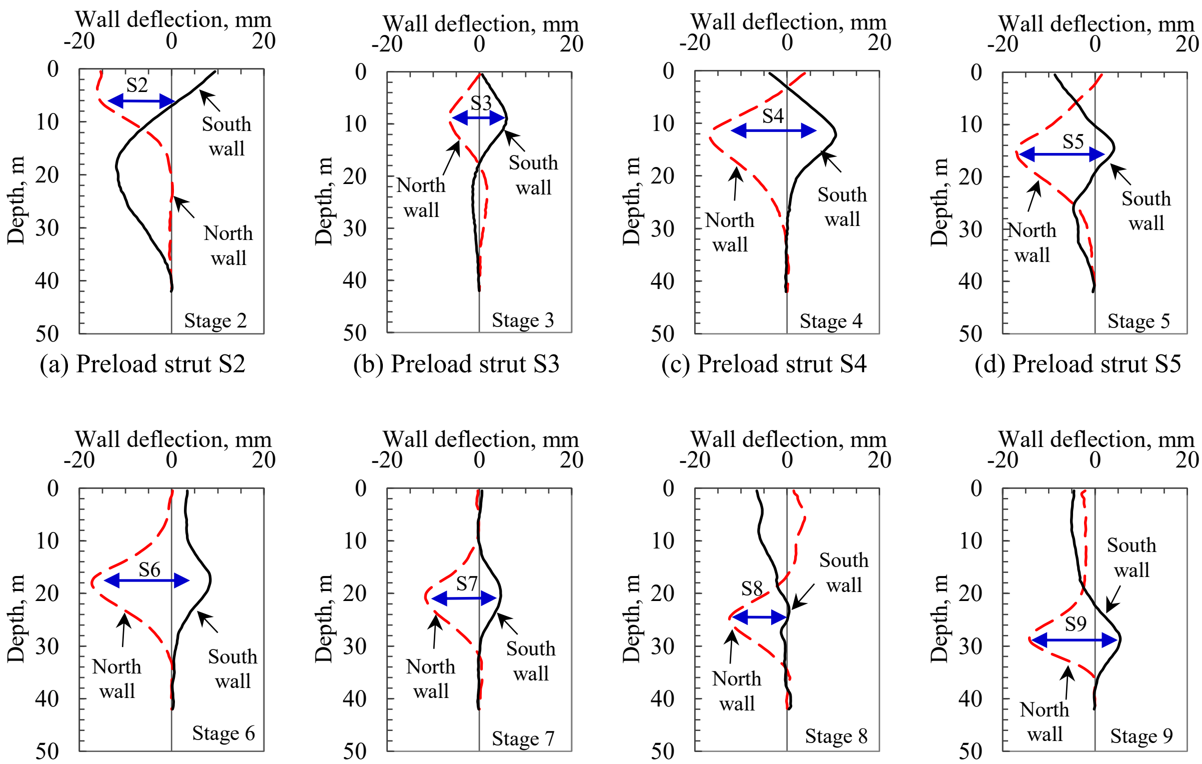

(a) Preload strut S2 (b) Preload strut S3 (c) Preload strut S4 (d) Preload strut S5

(e) Preload strut S6 (f) Preload strut S7 (g) Preload strut S8 (h) Preload strut S9

Proceedings DOI: 10.21467/proceedings.7.7
ISBN: 978-81-989164-3-3
Series: AIJR Proceedings
ISSN: 2582-3922

Figure 8: Wall deflections caused by struts preloading observed by the inclinometers at Section 11

Table 7: Wall deflections caused by struts preloading at Section 11

Strut	Depth m	Preload MN	Wall deflections, mm				Ratio of north wall deflection δ_n / δ
			Deduced from struts shortening, δ_w	Measured by inclinometers			
				South, δ_s	North, δ_n	Relative, δ	
S2	6.3	11.0	31	3	-16	19	0.84
S3	8.9	13.7	34	6	-6	12	0.50
S4	11.8	15.8	46	10	-17	27	0.63
S5	14.6	15.8	37	4	-17	21	0.81
S6	17.5	15.8	42	8	-17	25	0.68
S7	20.3	15.8	47	5	-12	17	0.71
S8	24.7	16.4	43	0	-12	12	1.00
S9	29.1	16.4	41	5	-14	19	0.74
Average			40	5.1	-13.9	19.0	0.74

4 LATERAL WALL DEFLECTIONS

4.1 Monitoring along undersea tunnel

Figure 9 to Figure 12 presents the inclinometer profiles along Section 11 to Section 14 of this undersea tunnel. The wall deflections occurred at the one side of the pipe pile wall were larger than those occurred on the opposite side. The differences in wall deflections were due to the imbalance of the earth pressures acting on the two walls. It is noted that in Figures 9 to 12, the wall deflections in positive and in negative values denote the southward and the northward wall movements respectively.

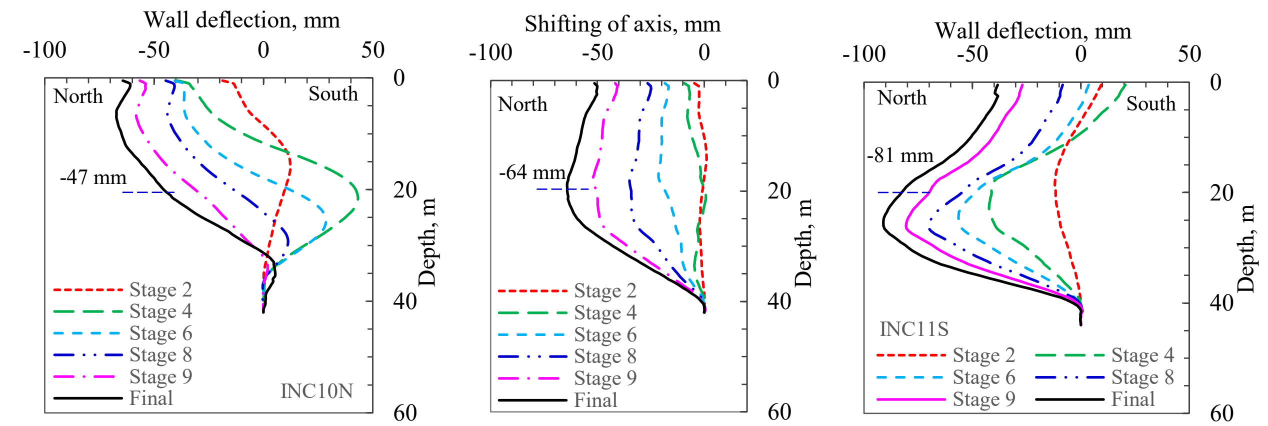

(a) North wall (b) Central axis (c) South wall

Figure 9: Observed wall deflection profiles at Section 11

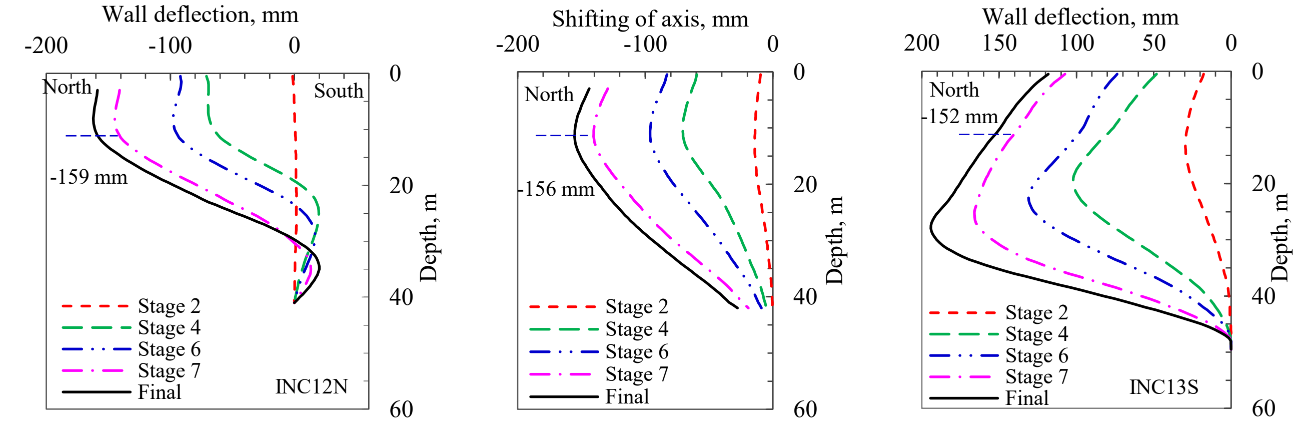

(a) North wall (b) Central axis (c) South wall

Figure 10: Observed wall deflection profiles at Section 12

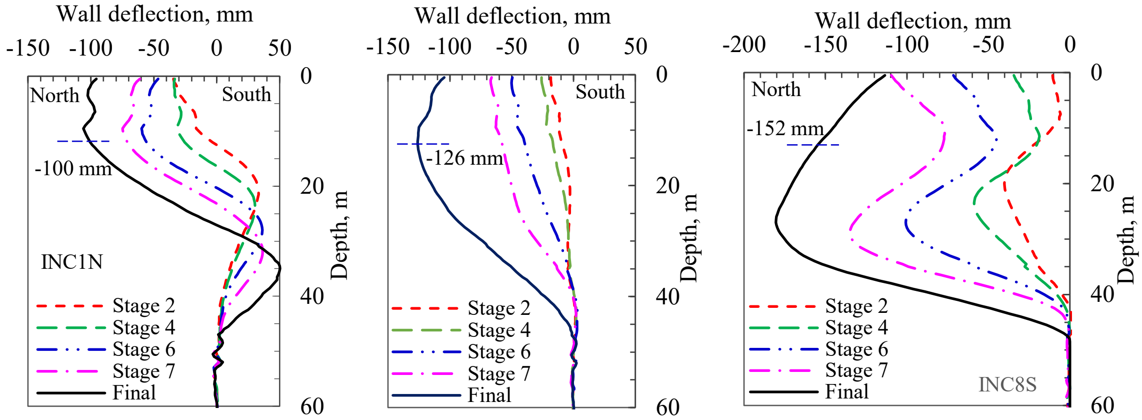

(a) North wall (b) Central axis (c) South wall

Figure 11: Observed wall deflection profiles at Section 13

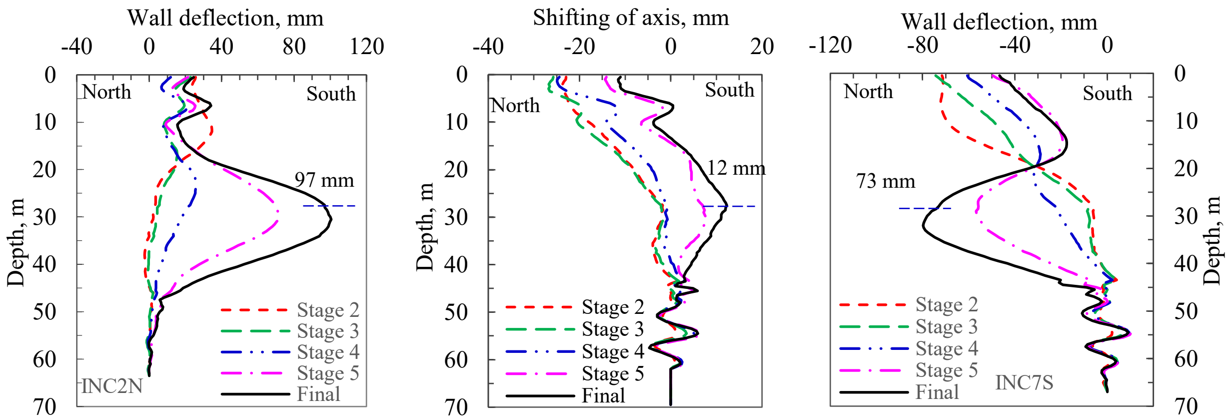

(a) North wall (b) Central axis (c) South wall

Figure 12: Observed wall deflection profiles at Section 14

Take Figure 9a as an example, there were inward wall movements occurring at the depths between 10 m and 30 m. However, the entire north wall was pushed backward. As a results, net outward wall movements occurred. Figure 9 shows that the maximum inward wall deflections on the south and the north wall in the final stage at Section 11 were -90.6 mm inward and -66 mm outward respectively. The north wall was pushed outward by the multi rows of struts under the active earth pressures acting behind the south wall. The earth pressure imbalance is further discussed in Section 5.1.

4.2 Fixation of the inclinometer toes

It is noted that the inclinometers were installed behind the pipe pile wall at the mid-point between two piles. The toe levels of the inclinometer casings were installed at least 2 m below the rockhead level so that in the interpretation of the inclinometer profiles, the toes of inclinometers can be taken as the fixed points. Table 2 summarizes the toes levels of the inclinometers installed at Section 11 to Section 14. The table shows that the embedment lengths of the inclinometer casings in rock ranged from 2 m to 20.7 m except inclinometer INC2N. At Section 14, the north pipe pile wall encountered the Granite IV at the level of -48 mPD. The toe of inclinometer INC2N was embedded in a core-boulder of 1.3 m in size above the rockhead. As such, the assumption for the inclinometers toes as the fixed point is valid for the inclinometers along the undersea tunnel.

Table 2 also shows that the pipe pile walls at Section 11, Section 12 and the north wall of Section 13 were penetrated 1.5 m to 7.0 m into the rockhead. The excavation level was 2 m below the rockhead at the north side of Section 11.

5 INFLUENCES OF EARTH-PRESSURE IMBALANCE

5.1 Shifting of the axis of excavation

The earth-pressure imbalance effect causes the asymmetrical performance of the wall deflection profiles of the walls on two sides of the excavation. Moh & Hwang (1997) reported the asymmetrical wall deflections at a basement excavation case located at the northern rim of the Taipei basin. Wong & Yong (2013) reported the earth-pressure imbalance effect for an excavation case for the Central Wanchai Bypass (CWB) cut-and-cover tunnel and in the Nicoll Highway case in Singapore.

The shifting of the central axes of the excavation trench in Section 11 to Section 14 are presented in Figure 9b, Figure 10b, Figure 11b and Figure 12b. The shifting of the central axis, δ_c, is defined as:

$$\delta_c = (\delta_1 + \delta_2) / 2 \qquad (1)$$

where the δ_1 and the δ_2 values are the deflections of the walls with the deeper and the shallower rockhead levels in the final stage respectively.

Table 8 summarized the shifting of the undersea tunnel along Section 11 to Section 14 and the depths to the rockhead levels on the north and the south walls in those sections. It is noted that the positive and the negative wall deflection values presented in Table 8 denote the southward and the northward movements respectively. The directions of the shifting of the central axis for Sections 11 to Section 13 had the same direction with those occurring at the north wall. The northward movements were caused by the shallower depths to the rockhead, the H_2 values, on the north side. For Section 14 where the inward wall movements occurred on both sides, the central axis shifted toward south, where the south wall had the shallower depth to the rockhead.

In Table 8, the H_1 and the H_2 values are the depths to the rockhead with the deeper and the shallower levels respectively. The central axis shifting values, δ_c, that obtained from Figure 9b to Figure 12b, vary from 12 mm to 156 mm in the final stage.

Table 8: Summary of central axis shifting in the final stage

Case	Location	Excavation depth H, m	Depth to rockhead			Wall deflection			Axis shift δ_c, mm
			Deep side H_1, m	Shallow side H_2, m	H_1/H_2 ratio	Depth, m	Deep side δ_1, mm	Shallow side δ_2, mm	
1 (This study)	Section 11	30.0	32.0	28.0	1.14	19.5	-81	-47	-64
	Section 12	33.1	44.0	34.5	1.27	11.0	-152	-159	-156
	Section 13	32.0	50.5	45.5	1.11	12.0	-152	-100	-126
	Section 14	25.7	59.2	59.0	1.00	28.0	97	-73	12
2	CWB tunnel	18.3	41.3	39.6	1.04	20.0	61.2	28.8	16.2
3	Taipei rim	23.3	38	15	2.53	19.0	198	5	97

5.2 Relationship of axis shift with excavation depths

Figures 9c, 10c and 11c show that the south wall had inward movements. The pressures acting on the south wall were in active state. On the opposite side, Figures 9a, 10a and 11a show that the north wall above the excavation levels in each stage had outward movements. The pressures acting on the north wall above the excavation levels were in the passive state and those below the excavation levels were in active state. The division line between the passive and the active state on the north wall propagated downward as excavation proceeded.

Figure 13 shows the relationship between the δ_c values against the excavation depths, the H values, for Section 11 to Section 14. The maximum axis shift values are approximately proportional to the excavation depths. The rates of increase in the shift values with the H values, the δ_c/H ratios, vary between various sections. It appears that the δ_c/H ratios would depend on the ratios of the depths to the rockhead levels on the two sides. The larger of the H_1/H_2 ratios, the steeper rate of increase in the shift values or the larger the δ_c/H ratios.

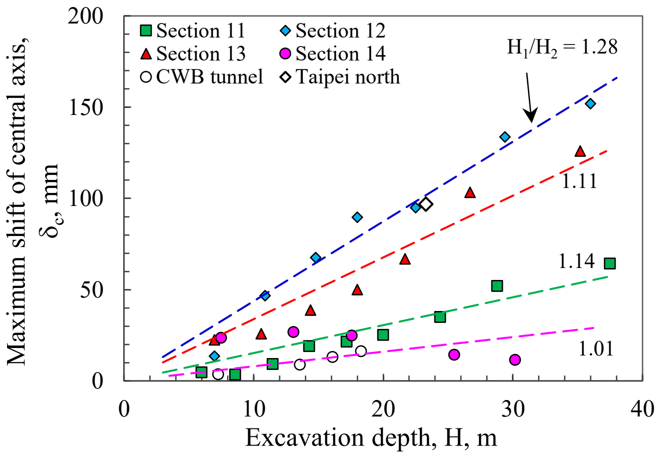

Figure 13: Relationship between excavation depths and the shifts of the central axes

5.3 Relationship of axis shift with depths to rockhead

Due to the uncertainties on the distribution and mobilization of the passive and active pressures on the wall with the outward movements, it is proposed that the variation of the δ_c/H ratios could be related to the H_1/H_2 ratios. The H_1/H_2 would be equivalent the ratio of the earth pressure acting on the two sides of the cofferdam. Figure 14 shows the relationship between the δ_c/H ratios against the H_1/H_2 ratios for Section 11 to Section 14. The δ_c/H ratios for the CWB tunnel and for the Taipei rim cases are included in the correlation. The set of δ_c/H versus H_1/H_2 ratios are fitted into the hyperbolic function that expressed in Equation 2:

$$\delta_c / H = (H_1/H_2 - 1) / [\alpha + \beta (H_1/H_2 - 1)] \quad (2)$$

with the coefficient $\alpha = 0.00002$ and $\beta = 0.00014$. The hyperbolic function of the relationship is an indication of the nonlinearity of the supporting ground. For the excavation Case 3 located at the northern rim of the Taipei Basin, the δ_c value is normalized with the H_2 value of 15 m because the depth to the shallower rockhead, H_2, is less than the excavation depth, H, of 23.3 m.

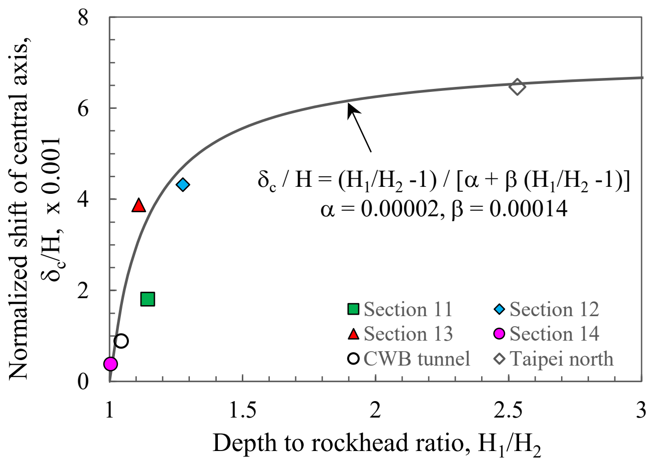

Figure 14: Relationship between depth to rockhead ratios and the normalized shift of the central axis

6 CONCLUSIONS

Based on the wall deflection profiles observed in inclinometers installed on opposite sides of the excavation trench of a cut-and-cover tunnel, the earth pressure imbalance effect has been observed. This issue is very complicated and can only be sorted out by numerical analyses. The following are the preliminary findings:

(1) Mainly due to the difference in the depths to the rockhead levels on both sides of the walls of the undersea tunnel, there is the earth-pressure imbalance effect causing differential lateral wall deflections. The wall on the shallower rockhead side was pushed back by the wall on the opposite side through the struts.
(2) The magnitude of the shifting of the central axis of the excavation trench is proportional to the excavation depths.
(3) The rate of increase in the axis shift values is proportional to the ratios between the depths to the deeper rockhead and the depths to the shallower rockhead levels on the two sides of the cofferdam.
(4) Based on the jack cylinder extension measurements in the preloading operation, the total wall deflections on the 2 sides of wall were around 40 mm measured immediately after locked-off with the shim plates.
(5) Inclinometers monitoring conducted on the following day of preloading showed that the wall movements occurring on the shallower rockhead side contributed around 3 quarter of the total wall deflections.

In the next study, numerical analysis shall be conducted to further examine the earth pressure imbalance effect to the performance of asymmetrical wall deflections. The effects due to wall stiffnesses and the magnitude of the preload are the subjects to be studied.

With the proper understanding the mechanism causing the asymmetrical wall deflections due to the effect of earth pressure imbalance, the design and construction of the underground infrastructures could be refined and the cost-effective solutions to engineering challenges could be formulated.

REFERENCES

Moh, Z.C. & Hwang, R.N. 1997. Geotechnical problems related to design and construction of the Taipei Transit Systems. *Proc. of Keynote Speech, Professor Chun Fung Kee Memorial Lecture*, September 6, 1997, Kuala Lumpur, Malaysia.

Wong, L.W. & Yong, C.C. 2013. Earth pressure imbalance on deep excavation. *Advance in Geotechnical Infrastructure, 18th Southeast Asian Geotechnical Conference*, May, Singapore: 275-281.